Letter

Josephson effect as a signature of electron-hole superfluidity in bilayers of van der Waals heterostructures

Filippo Pascucci,[1,2] Sara Conti,[3] David Neilson,[3] Jacques Tempere,[2] and Andrea Perali[1,*]
[1]*Supernano Laboratory, School of Pharmacy, University of Camerino, 62032 Camerino (MC), Italy*
[2]*TQC, University of Antwerp, Universiteitsplein 1, 2610 Antwerp, Belgium*
[3]*CMT, Department of Physics, University of Antwerp, Groenenborgerlaan 171, 2020 Antwerp, Belgium*

(Received 13 May 2022; revised 23 November 2022; accepted 28 November 2022; published 19 December 2022)

We investigate a Josephson junction in an electron-hole superfluid in a double-layer transition metal dichalcogenide heterostructure. The observation of a critical tunneling current is a clear signature of superfluidity. In addition, we find the BCS-BEC crossover physics in the narrow barrier region controls the critical current across the entire system. The corresponding critical velocity, which is measurable in this system, has a maximum when the excitations pass from bosonic to fermionic. Remarkably, this occurs for the density at the boundary of the BEC to BCS-BEC crossover regime determined from the condensate fraction. This provides, in a semiconductor system, an experimental way to determine the position of this boundary.

DOI: 10.1103/PhysRevB.106.L220503

Recent experimental reports of quantum condensation with bound pairs of spatially separated electrons and holes in double layers of graphene [1] or transition metal dichalcogenide (TMD) van der Waals heterostructures [2], have created a flurry of new experimental and theoretical investigations. Spatially separating the electrons and holes prevents them from recombining, opening the way to a low-temperature stable, long-lived superfluid [3–6]. By varying the equal carrier densities in the two layers using metal gates, the superfluid can be tuned from the strongly coupled Bose-Einstein condensation (BEC) regime of compact bosonlike particles to an intermediate-coupling regime, and to the Bardeen-Cooper-Schrieffer (BCS) regime with more extended fermionic pairs [7–9].

From an application viewpoint, a supercurrent in an electron-hole superfluid can carry a particle flow without dissipation. A current is independently injected in each layer with opposite directions in order to have a stable dissipationless exciton current and avoid the electron-hole recombination [10]. This directly leads to applications in dissipationless solid-state electronics [10,11].

Up to now, proving a superfluid phase in exciton systems has required painstaking analysis to merge Coulomb drag resistance and counterflow experimental data [12]. On the one hand, Coulomb drag [13–15] and interlayer tunneling experiments [1,16] allow us to prove the presence of excitons, and on the other hand, counterflow measurements [10,17] can reveal dissipationless current in the system. Observing the presence of excitons or the nondissipative counterflow current by themselves is not sufficient to claim superfluidity. The neutrality of the electron-hole pairs creates a challenge to unambiguously identify the fluid as a superfluid [10]. The conventional criterion to identify superconductivity, the combination of perfect conduction and the Meissner effect (perfect diamagnetism), cannot be used with neutral pairs.

Here, we propose that the Josephson effect [18–21] can provide an unambiguous signal of the electron-hole superfluidity. In a Josephson junction, two superfluids are separated by a thin potential barrier, and a phase difference between the superfluids leads to a steady current flow. The observation of a dissipationless current through the barrier when there is no driving potential present is regarded as an optimal direct experimental way to confirm the existence of the single amplitude and phase of the macroscopic wave function that characterizes a quantum condensed state [22,23].

We find that the maximum value of the dissipationless current exhibits a notable sensitivity to the bosonic or fermionic nature of the low-lying excitations of the superfluid state in the barrier region. We further show that this sensitivity can be exploited to identify and distinguish in the barrier region, the BEC regime of bosoniclike pairs from the weakly bound fermion pairs of the BCS-BEC crossover and BCS regimes [24].

The Josephson junction can be fabricated using a combination of lateral stitching and vertical stacking of TMD heterostructures [25–27], as represented in Fig. 1(a). A vertical stacking of two different TMD monolayers, TMD_1 and TMD_2, is separated by a thin barrier made of two different undoped TMD monolayers, TMD_3 and TMD_4. The potential barrier height is determined by the difference in energy of the conduction (valence) bands in the doped TMDs and in the undoped TMDs of the barrier [28].

The critical Josephson current can be measured in a counterflow configuration [10], using the method of Anderson [29] and Shapiro [30]. Unlike in superconductors, the total superfluid current is neutral. However, the excitons are formed by charged particles, thus the independent currents injected in the two layers are not neutral and they are dissipationless in the

*Corresponding author: andrea.perali@unicam.it

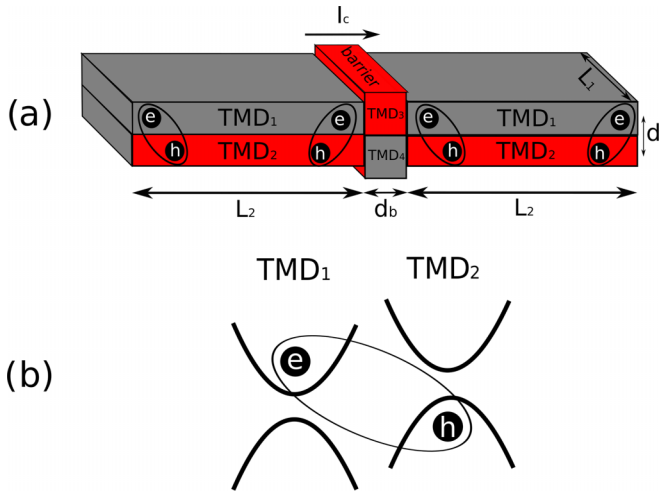

FIG. 1. (a) Schematic of Josephson junction with the different layers labeled TMD_1–TMD_4. d is the layer separation, d_b the barrier thickness, and L_1 and L_2 the transverse and longitudinal layer lengths. Electron-hole pairs are shown. (b) Energy band alignments at the type-II TMD_1/TMD_2 interface.

superfluid phase. Here, it is this single-layer current that is used to study the current-voltage characteristic. Increasing the current injected, the maximum current for which the voltage drop is zero corresponds to the critical Josephson current. The advantage of this proposal with respect to Ref. [12] is that a counterflow measure of the Josephson current is enough to claim the superfluid phase without the necessity for the Coulomb drag experiment.

We select the TMD_1 and TMD_2 of the vertical stacking to have a type-II interface, with the edges of the conduction and valence band at different energies [Fig. 1(b)]. This keeps the electrons and holes spatially separate without the need for an insulating barrier. We consider a single band with one interaction channel.

The coupled BCS mean-field equations for the superfluid gap Δ_k and density n [31] remain a good approximation in the BCS-BEC crossover and BEC regimes at zero temperature also in two dimensions (2D) [32,33],

$$\Delta_k = -\frac{1}{L_1 L_2}\sum_{k'} \mathcal{F}_{1,2} V^{\rm sc}_{k-k'} \frac{\Delta_{k'}}{2E_{k'}}, \tag{1}$$

$$n = \frac{g_s}{L_1 L_2}\sum_k \frac{1}{2}\left(1 - \frac{\varepsilon_k - \mu_s}{E_k}\right). \tag{2}$$

We set the electron and hole densities n equal, and take equal effective masses m^* in the TMD single-particle parabolic bands $\varepsilon_k = \hbar^2 k^2/2m^*$. The excitation energy $E_k = \sqrt{\xi_k^2 + \Delta_k^2}$, with $\xi_k = \varepsilon_k - \mu_s$ and μ_s the single-particle chemical potential. The form factor $\mathcal{F}_{1,2}$ accounts for the overlap between the single-particle wave functions in TMD_1 and TMD_2. The spin degeneracy is $g_s = 2$, and L_1 and L_2 the transverse and longitudinal layer lengths.

In Eq. (1), $V^{\rm sc}_{k-k'}$ is the effective self-consistent screened Coulomb attraction between electrons and holes. Because of the long-range nature of Coulomb interactions, screening plays a crucial role here [34]. We use the expression in Ref. [31], which self-consistently takes into account the weakening of the screening in the presence of a superfluid energy gap,

$$V^{\rm sc}_{\mathbf{q}} = \frac{V^D_{\mathbf{q}}}{1 - 2V^S_{\mathbf{q}}[\Pi_n(\mathbf{q}) + \Pi_a(\mathbf{q})] + \mathcal{A}_{\mathbf{q}}\mathcal{B}_{\mathbf{q}}}. \tag{3}$$

$V^S_{\mathbf{q}}$ and $V^D_{\mathbf{q}}$ are the bare Coulomb interactions within a layer and between layers, respectively. $\Pi_n(\mathbf{q})$ and $\Pi_a(\mathbf{q})$ are the normal and anomalous polarizabilities. For brevity, in Eq. (3) we write $\mathcal{A}_{\mathbf{q}} = (V^S_{\mathbf{q}})^2 - (V^D_{\mathbf{q}})^2$ and $\mathcal{B}_{\mathbf{q}} = \Pi_n^2(\mathbf{q}) - \Pi_a^2(\mathbf{q})$.

The critical velocity of the superfluid is given by the Landau criterion [35],

$$v_c = \min_k \frac{\mathcal{E}_k}{\hbar k}. \tag{4}$$

There are two types of excitation energy $\mathcal{E}_k$ in this system, Anderson-Bogoliubov modes [36] associated with the bosonic behavior of the pairs, and the fermionic modes associated with pair-breaking excitations [37].

In the bosonic excitation branch, $\mathcal{E}_k$ is given by the dispersion relation $\mathcal{E}_k = \sqrt{\hbar^2 c_{\rm sf}^2 k^2 + \varepsilon_k^2}$ [37,38], where $c_{\rm sf} = \sqrt{\mu_{\rm sf}/2m}$ [39] is the speed of sound, with superfluid chemical potential $\mu_{\rm sf} = 2\mu_s + \varepsilon_B$, and ε_B the binding energy of a single electron-hole pair. From Eq. (4), the critical velocity for bosonic excitations is thus the speed of sound,

$$v_c^{\rm (BEC)} = c_{\rm sf} = \sqrt{\frac{\mu_{\rm sf}}{2m}}. \tag{5}$$

Instead, for single-particle fermionic excitations $\mathcal{E}_k = E_k = \sqrt{\xi_k^2 + \Delta_k^2}$, and the critical velocity is the pair-breaking (p-b) velocity [37],

$$v_c^{\rm (p\text{-}b)} = \min_k \frac{\sqrt{(\varepsilon_k - \mu_s)^2 + \Delta_k^2}}{\hbar k}, \tag{6}$$

is numerically evaluated for given values of μ_s and Δ_k to determine the value of $k = k_{\rm min}$ that minimizes Eq. (6). As the density is increased and the superfluid regimes are scanned from BEC to BCS-BEC crossover to BCS, the critical velocity should switch from $v_c^{\rm (BEC)}$ to $v_c^{\rm (p\text{-}b)}$, whichever is the lesser.

We consider only sufficiently wide barriers for the Thomas-Fermi local approximation to be valid, $d_b > \xi$, where $\xi = \hbar/mv_c$ is the superfluid coherence length [37,40]. In the barrier region, the single-particle chemical potential μ_s^b and the superfluid chemical potential $\mu_{\rm sf}^b$ will be reduced compared with their values outside the barrier,

$$\mu_s^b = \mu_s - V_0,$$
$$\mu_{\rm sf}^b = \mu_{\rm sf} - 2V_0 = 2(\mu_s - V_0) + \varepsilon_B. \tag{7}$$

Using μ_s^b in Eqs. (1) and (2) gives the superfluid gap Δ_k^b and the density n^b inside the barrier region. For a low rectangular potential barrier, $V_0 < \mu_{sf}/2$, current can flow over the barrier across a superfluid region in the barrier with density $n^b < n$. For high potential barriers, $V_0 \geqslant \mu_{\rm sf}/2$, $\mu_s^b < -\varepsilon_B/2$, and $n^b = 0$, so the current across the barrier is given purely by quantum tunneling of the electron-hole pairs [41,42].

Figure 2(a) shows for different barrier heights V_0 in the low barrier regime, the superfluid density in the barrier n^b

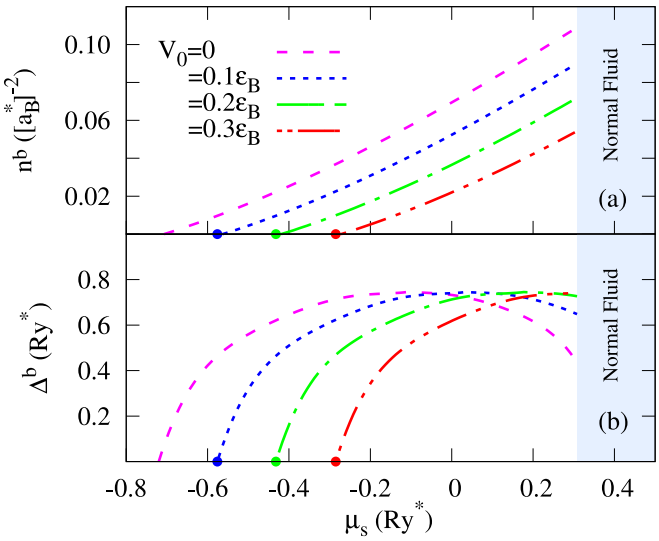

FIG. 2. (a) Density n^b inside the barrier as a function of the single-particle chemical potential μ_s outside the barrier. V_0 is the barrier height with $\varepsilon_B = 1.42$ Ry*. In the shaded area, strong screening suppresses the superfluidity. (b) Superfluid gap Δ^b inside the barrier. The n^b and Δ^b have been calculated using μ_s^b in Eqs. (1) and (2).

as a function of the μ_s outside the barrier. We use effective Rydbergs Ry* for the energy scale and effective Bohr radii a_B^* for the length scale. Table I gives values for Ry* and a_B^* for different TMD heterostructures to connect with experimental results. For $d = 0.6$ nm, the typical layer separation of a TMD type-II interface, $\varepsilon_B = 1.42$ Ry*. The color-coded dots indicate the value $\mu_s = -\varepsilon_B/2 + V_0$ below which n^b is zero. The BEC regime is characterized by negative values of μ_s. As μ_s increases and becomes positive, the system enters the BCS-BEC crossover regime, but μ_s remains well below the Fermi energy. Only in the weak-coupled BCS limit would μ_s approach the Fermi energy. However, for sufficiently large μ_s, strong screening of the electron-hole pair interaction in the superfluid outside the barrier region suppresses the superfluidity leading to a first-order phase transition in the mean-field approximation [31] (the shaded regions in Fig. 2). The $V_0 = 0$ curve in Fig. 2(a) gives as a reference the superfluid density n in the absence of a barrier. This reaches a maximum at the value $\mu_s = 0.31$ Ry* for density $n = n^b = 0.105(a_B^*)^{-2}$. This defines the onset density n_0 for the superfluidity.

Figure 2(b) shows the maximum of the superfluid gap Δ^b inside the barrier as a function of μ_s. The curve for $V_0 = 0$ also gives the maximum of the superfluid gap Δ_k in the superfluid regions outside any barrier and, as n, this gap vanishes when μ_s reaches $-\varepsilon_B/2$. For $V_0 > 0$, Δ^b for the barrier vanishes at the same value of μ_s at which n^b vanishes.

The barrier height V_0 can be varied by suitable material choice of TMDs with type-II interfaces. Table I gives examples. As a final example, $WS_2|WSe_2$—$MoSe_2|WSe_2$, the barrier is inserted only in the electron monolayer, a configuration which may be more straightforward to fabricate.

For low potential barriers $V_0 < \mu_{sf}/2$ there is significant superfluid flow over the barrier. The critical current in the barrier region is

$$I_c^b = n^b L_1 v_c^b. \tag{8}$$

The critical velocity v_c^b in the barrier is the lesser of $v_c^{b(\mathrm{BEC})}$ and $v_c^{b(\mathrm{p\text{-}b})}$, obtained from Eqs. (5) and (6) with μ_{sf}^b and Δ_k^b.

For high potential barriers, $V_0 > \mu_{sf}/2$, quantum tunneling of the electron-hole pairs through the barrier determines the critical current [42],

$$\hbar I_c^b = n_c\, t_{sf}(\mu_{sf}) L_1 L_2. \tag{9}$$

$n_c = \mathcal{C}n$ is the density of the superfluid condensate, with $\mathcal{C}$ the condensate fraction of the superfluid state, which can be calculated as [43,44]

$$\mathcal{C} = \frac{\sum_k u_k^2 v_k^2}{\sum_k v_k^2} = \frac{1}{2n}\sum_k \frac{\Delta_k^2}{E_k^2}. \tag{10}$$

Replacing in Eq. (10) Δ_k^b, n^b, and μ_s^b, it is possible to obtain the condensate fraction $\mathcal{C}^b$ in the barrier region for the low potential barrier. The transfer matrix element [41],

$$t_{sf}(\mu_{sf}) = f(V_0/\mu_{sf})\frac{\mu_{sf}}{k_{\mu_{sf}} L_1} e^{-k_{\mu_{sf}} d_b}, \tag{11}$$

is the probability for an electron-hole pair to tunnel across the barrier, where $k_{\mu_{sf}}^{-1} = \hbar/\sqrt{2m(V_0 - \mu_{sf})}$ is the wave-function decay length in the barrier, and the expression for $f(V_0/\mu_{sf})$ was derived in Ref. [41],

$$f(V_0/\mu_{sf}) = \left[1 - \frac{V_0}{\mu_{sf}} - \sqrt{\left(\frac{V_0}{\mu_{sf}}\right)^2 - 1}\right]^2. \tag{12}$$

So for $V_0 > \mu_{sf}/2$, the final expression for the critical current is

$$I_c^b = \frac{n_c\, \mu_{sf} f(V_0/\mu_{sf}) e^{-k_{\mu_{sf}} d_b} L_2}{\hbar k_{\mu_{sf}}}. \tag{13}$$

TABLE I. Material parameters and barrier heights V_0. The V_0 has been calculated by the difference in energy of the conduction (valence) bands in the doped TMDs and in the undoped TMDs of the barrier [28].

$TMD_1\|TMD_2$	–	$TMD_3\|TMD_4$	a_B^* (nm)	Ry* (meV)	ε_B (meV)	V_0 (ε_B)
$MoS_2\|MoSe_2$	–	$MoSe_2\|WSe_2$	1.3	100	140	0.04
$MoS_2\|WSe_2$	–	$MoTe_2\|WTe_2$	1.7	77	108	0.05
$WS_2\|WSe_2$	–	$MoTe_2\|MoTe_2$	1.8	71	99	0.10
$MoS_2\|WS_2$	–	$WS_2\|MoSe_2$	1.7	77	108	0.20
$MoSe_2\|MoTe_2$	–	$MoS_2\|MoSe_2$	1.1	116	162	0.33
$MoS_2\|MoSe_2$	–	$WTe_2\|WSe_2$	1.3	100	140	0.71
$WS_2\|WSe_2$	–	$MoSe_2\|WSe_2$	1.9	71	99	0.33

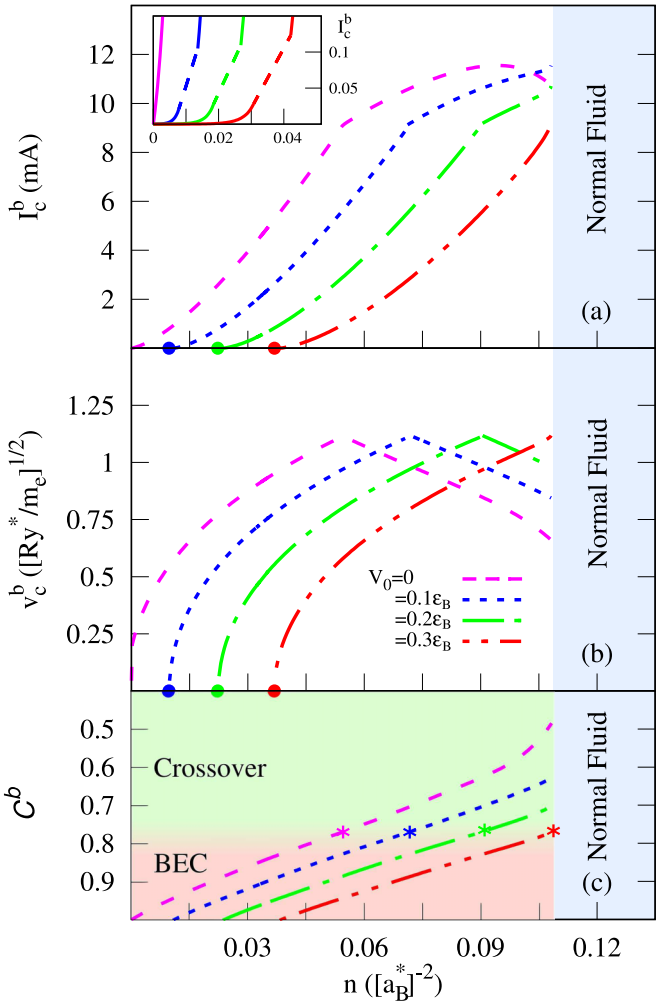

FIG. 3. (a) Critical current I_c obtained with Eq. (8) in the barrier for barrier height V_0, as a function of density n. Inset: Details of the critical current at very low densities; continuous lines in the upper part of the inset are a zoom-in of (a), the continuous line in the lower part of the inset obtained with Eq. (13), and dashed lines interpolate high barrier and low barrier results. (b) Critical velocity v_c^b in the barrier [Eq. (4)]. (c) Condensate fraction C^b in the barrier [Eq. (10)]. The asterisk symbols in (c) match the position of the maximum of the critical velocity v_c^b in (b).

Figure 3(a) shows the critical current in the barrier I_c^b as a function of the density n outside the barrier. The colored dots again mark the value of n at which n_b drops to zero and the switch occurs from predominantly flow over to tunneling. The inset shows in detail the critical current in the tunneling region. This is seen to connect smoothly (dashed lines) with the critical current in the flow over region. We recall that the existence of a nonzero tunneling current in this region is accepted as a clear signature of superfluidity. The flattening of I_c^b at high densities reflects the drop in Δ_k^b from the strong screening [Fig. 2(b)].

We note that I_c^b is everywhere less than the critical current outside the barrier $I_c = nL_2 v_c$, shown by the $V_0 = 0$ curve. For this reason, the overall critical current in the system is given by I_c^b. Thus the BCS-BEC crossover physics in the barrier region controls the transport properties of the entire device.

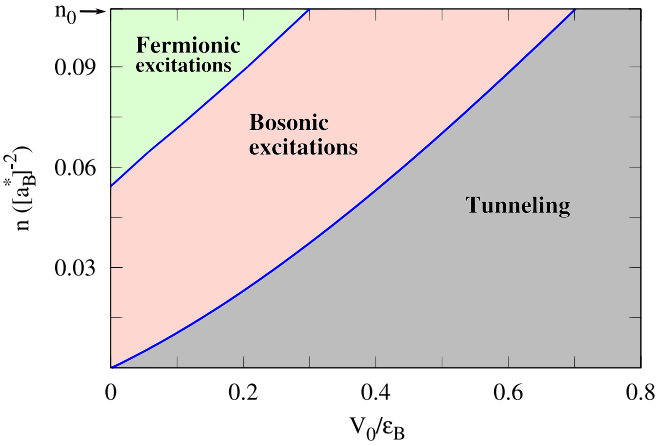

FIG. 4. Driving mechanisms for the Josephson critical current at different barrier heights V_0. In the fermionic excitation area the critical current is determined by the pair-breaking branch, and in the bosonic excitation area it is determined by the Anderson-Bogoliubov branch. The tunneling area corresponds to the high potential barrier regime.

Figure 3(b) shows the critical velocity v_c^b across the barrier. The maxima in v_c^b result from the switch from Anderson-Bogoliubov bosonic excitations to single-particle fermionic excitations, $v_c^{(\text{p-b})}$ increasing with density while $v_c^{(\text{BEC})}$ decreases with density [45]. As expected, the positions of the maxima are sensitive to the barrier height. Figure 3(c) shows that the maximum of v_c^b for each value of V_0 matches the density at which the condensate fraction $C^b = 0.8$. Remarkably, this value agrees with the conventional criterion used to identify the crossover to the BEC boundary given by the vanishing of the single-particle chemical potential [9,46]. It is an attractive concept and relevant for experiments, that the switchover from bosonic excitations to single-particle fermionic excitations lines up with the BEC and BCS-BEC crossover regime boundary. In contrast to the condensate fraction which is not observable, the critical velocity $v_c^b = I_c^b/n$ is a directly experimentally measurable quantity in these electron-hole Josephson devices: $I_c^b = I_c$, the overall critical current of the system, and the density n is precisely controlled by gate potentials. This remarkable result provides a way of experimentally locating the BCS-BEC crossover boundary in 2D exciton systems.

In Fig. 4, we show the nature of the driving mechanisms of I_c^b for different V_0 and n. The density n is capped at the superfluid onset density n_0. For very small V_0, as we increase density, we go from bosonic excitations to fermionic pair-breaking excitations. On increasing V_0, a region of tunneling of electron-hole pairs appears at small n. When $V_0 > 0.3\varepsilon_B$, strong screening preempts v_c^b from reaching the maximum, so there are no pair-breaking fermionic excitations. For high potential barriers, $V_0 > 0.7\varepsilon_B$, there are no bosonic excitations, and only tunneling through the barrier remains.

We have demonstrated that measurements of the critical current across a Josephson-junction barrier can yield significant additional information on electron-hole superfluid properties in a double-layer TMD heterostructure. The barrier

can be fabricated and its height adjusted by suitable combinations of TMD layers. The additional information is as follows. (i) The existence of a Josephson effect below a critical tunneling current is *per se* a direct signature of superfluidity. We note that this could be used to distinguish between a phase of excitons in a normal or superfluid state. Up to now, this has required painstaking analysis to merge Coulomb drag resistance and counterflow experimental data [12]. (ii) For low barriers, the crossover physics in the barrier region controls the transport properties of the entire device. (iii) One can experimentally observe the maximum of the critical velocity at the density where excitations switch from bosonic to fermionic, the density in this system controlling the coupling strength. This maximum can be used to identify the boundary separating the BEC and BCS-BEC crossover regimes of the electron-hole superfluidity, and in fact, remarkably, the density at the maximum matches the density at which the condensate fraction passes through 0.8.

The work was partially supported by the projects G061820N, G060820N, G0H1122N, and by the Flemish Science Foundation (FWO-Vl).

[1] G. W. Burg, N. Prasad, K. Kim, T. Taniguchi, K. Watanabe, A. H. MacDonald, L. F. Register, and E. Tutuc, Strongly Enhanced Tunneling at Total Charge Neutrality in Double-Bilayer Graphene-WSe_2 Heterostructures, Phys. Rev. Lett. **120**, 177702 (2018).

[2] Z. Wang, D. A. Rhodes, K. Watanabe, T. Taniguchi, J. C. Hone, J. Shan, and K. F. Mak, Evidence of high-temperature exciton condensation in two-dimensional atomic double layers, Nature (London) **574**, 76 (2019).

[3] Y. E. Lozovik and V. I. Yudson, A new mechanism for superconductivity: Pairing between spatially separated electrons and holes, Zh. Eksp. Teor. Fiz. **71**, 738 (1976) [Sov. Phys. JETP **44**, 389 (1976)].

[4] L. Ma, P. X. Nguyen, Z. Wang, Y. Zeng, K. Watanabe, T. Taniguchi, A. H. MacDonald, K. F. Mak, and J. Shan, Strongly correlated excitonic insulator in atomic double layers, Nature (London) **598**, 585 (2021).

[5] Y. Zeng and A. H. MacDonald, Electrically controlled two-dimensional electron-hole fluids, Phys. Rev. B **102**, 085154 (2020).

[6] M. Xie and A. H. MacDonald, Electrical Reservoirs for Bilayer Excitons, Phys. Rev. Lett. **121**, 067702 (2018).

[7] P. Pieri, D. Neilson, and G. C. Strinati, Effects of density imbalance on the BCS-BEC crossover in semiconductor electron-hole bilayers, Phys. Rev. B **75**, 113301 (2007).

[8] L. Salasnich, P. A. Marchetti, and F. Toigo, Superfluidity, sound velocity, and quasicondensation in the two-dimensional BCS-BEC crossover, Phys. Rev. A **88**, 053612 (2013).

[9] P. López Ríos, A. Perali, R. J. Needs, and D. Neilson, Evidence from Quantum Monte Carlo Simulations of Large-Gap Superfluidity and BCS-BEC Crossover in Double Electron-Hole Layers, Phys. Rev. Lett. **120**, 177701 (2018).

[10] J.-J. Su and A. H. MacDonald, How to make a bilayer exciton condensate flow, Nat. Phys. **4**, 799 (2008).

[11] D. Nandi, A. D. K. Finck, J. P. Eisenstein, L. N. Pfeiffer, and K. W. West, Exciton condensation and perfect Coulomb drag, Nature (London) **488**, 481 (2012).

[12] X. Liu, J. I. A. Li, K. Watanabe, T. Taniguchi, J. Hone, B. I. Halperin, P. Kim, and C. R. Dean, Crossover between strongly coupled and weakly coupled exciton superfluids, Science **375**, 205 (2022).

[13] B. N. Narozhny and A. Levchenko, Coulomb drag, Rev. Mod. Phys. **88**, 025003 (2016).

[14] J. I. A. Li, T. Taniguchi, K. Watanabe, J. Hone, A. Levchenko, and C. R. Dean, Negative Coulomb Drag in Double Bilayer Graphene, Phys. Rev. Lett. **117**, 046802 (2016).

[15] J. A. Seamons, C. P. Morath, J. L. Reno, and M. P. Lilly, Coulomb Drag in the Exciton Regime in Electron-Hole Bilayers, Phys. Rev. Lett. **102**, 026804 (2009).

[16] I. B. Spielman, J. P. Eisenstein, L. N. Pfeiffer, and K. W. West, Resonantly Enhanced Tunneling in a Double Layer Quantum Hall Ferromagnet, Phys. Rev. Lett. **84**, 5808 (2000).

[17] E. Tutuc, M. Shayegan, and D. A. Huse, Counterflow Measurements in Strongly Correlated GaAs Hole Bilayers: Evidence for Electron-Hole Pairing, Phys. Rev. Lett. **93**, 036802 (2004).

[18] B. D. Josephson, Possible new effects in superconductive tunnelling, Phys. Lett. **1**, 251 (1962).

[19] B. Zenker, H. Fehske, and H. Beck, Excitonic Josephson effect in double-layer graphene junctions, Phys. Rev. B **92**, 081111(R) (2015).

[20] K. Ziegler, A. Sinner, and Y. E. Lozovik, Anomalous Josephson Effect of *s*-wave Pairing States in Chiral Double Layers, Phys. Rev. Lett. **128**, 157001 (2022).

[21] K. Park and S. Das Sarma, Coherent tunneling in exciton condensates of bilayer quantum Hall systems, Phys. Rev. B **74**, 035338 (2006).

[22] F. Ancilotto, L. Salasnich, and F. Toigo, dc Josephson effect with Fermi gases in the Bose-Einstein regime, Phys. Rev. A **79**, 033627 (2009).

[23] A. Spuntarelli, P. Pieri, and G. C. Strinati, Josephson Effect throughout the BCS-BEC Crossover, Phys. Rev. Lett. **99**, 040401 (2007).

[24] F. Pascucci and L. Salasnich, Josephson effect with superfluid fermions in the two-dimensional BCS-BEC crossover, Phys. Rev. A **102**, 013325 (2020).

[25] H. Taghinejad, A. A. Eftekhar, and A. A. Dibi, Lateral and vertical heterostructures in two-dimensional transition-metal dichalcogenides, Opt. Mater. Express **9**, 1590 (2019).

[26] M. Mahjouri-Samani, M.-W. Lin, K. Wang, A. R. Lupini, J. Lee, L. Basile, A. Boulesbaa, C. M. Rouleau, A. A. Puretzky, I. N. Ivanov, K. Xiao, M. Yoon, and D. B. Geohegan, Patterned arrays of lateral heterojunctions within monolayer two-dimensional semiconductors, Nat. Commun. **6**, 7749 (2015).

[27] R. Frisenda, E. Navarro-Moratalla, P. Gant, D. Pérez De Lara, P. Jarillo-Herrero, R. V. Gorbachev, and A. Castellanos-Gomez, Recent progress in the assembly of nanodevices and van der Waals heterostructures by deterministic placement of 2D materials, Chem. Soc. Rev. **47**, 53 (2018).

[28] C. Gong, H. Zhang, W. Wang, L. Colombo, R. M. Wallace, and K. Cho, Band alignment of two-dimensional transition metal

dichalcogenides: Application in tunnel field effect transistors, Appl. Phys. Lett. **107**, 139904 (2015).

[29] P. W. Anderson and J. M. Rowell, Probable Observation of the Josephson Superconducting Tunneling Effect, Phys. Rev. Lett. **10**, 230 (1963).

[30] S. Shapiro, Josephson Currents in Superconducting Tunneling: The Effect of Microwaves and Other Observations, Phys. Rev. Lett. **11**, 80 (1963).

[31] A. Perali, D. Neilson, and A. R. Hamilton, High-Temperature Superfluidity in Double-Bilayer Graphene, Phys. Rev. Lett. **110**, 146803 (2013).

[32] J. P. A. Devreese, J. Tempere, and C. A. R. Sá de Melo, Effects of Spin-Orbit Coupling on the Berezinskii-Kosterlitz-Thouless Transition and the Vortex-Antivortex Structure in Two-Dimensional Fermi Gases, Phys. Rev. Lett. **113**, 165304 (2014).

[33] L.-P. Lumbeeck, J. Tempere, and S. Klimin, Dispersion and damping of phononic excitations in Fermi superfluid gases in 2D, Condensed Matter **5**, 13 (2020).

[34] D. Neilson, A. Perali, and A. R. Hamilton, Excitonic superfluidity and screening in electron-hole bilayer systems, Phys. Rev. B **89**, 060502(R) (2014).

[35] L. Landau, Theory of the superfluidity of Helium II, Phys. Rev. **60**, 356 (1941).

[36] P. W. Anderson, Random-phase approximation in the theory of superconductivity, Phys. Rev. **112**, 1900 (1958).

[37] R. Combescot, M. Y. Kagan, and S. Stringari, Collective mode of homogeneous superfluid Fermi gases in the BEC-BCS crossover, Phys. Rev. A **74**, 042717 (2006).

[38] N. N. Bogoliubov, On the theory of superfluidity, J. Phys. (USSR) **11**, 23 (1947).

[39] L. Salasnich and F. Toigo, Composite bosons in the two-dimensional BCS-BEC crossover from Gaussian fluctuations, Phys. Rev. A **91**, 011604(R) (2015).

[40] S. Giorgini, L. P. Pitaevskii, and S. Stringari, Theory of ultracold atomic Fermi gases, Rev. Mod. Phys. **80**, 1215 (2008).

[41] F. Meier and W. Zwerger, Josephson tunneling between weakly interacting Bose-Einstein condensates, Phys. Rev. A **64**, 033610 (2001).

[42] M. Zaccanti and W. Zwerger, Critical Josephson current in BCS-BEC–crossover superfluids, Phys. Rev. A **100**, 063601 (2019).

[43] S. Giorgini, L. P. Pitaevskii, and S. Stringari, Condensate fraction and critical temperature of a trapped interacting Bose gas, Phys. Rev. A **54**, R4633 (1996).

[44] L. Salasnich, N. Manini, and A. Parola, Condensate fraction of a Fermi gas in the BCS-BEC crossover, Phys. Rev. A **72**, 023621 (2005).

[45] D. E. Miller, J. K. Chin, C. A. Stan, Y. Liu, W. Setiawan, C. Sanner, and W. Ketterle, Critical Velocity for Superfluid Flow across the BEC-BCS Crossover, Phys. Rev. Lett. **99**, 070402 (2007).

[46] A. Guidini and A. Perali, Band-edge BCS–BEC crossover in a two-band superconductor: Physical properties and detection parameters, Supercond. Sci. Technol. **27**, 124002 (2014).